HHS Public Access

Author manuscript

Nanomedicine. Author manuscript; available in PMC 2018 July 01.

Published in final edited form as:

Nanomedicine. 2017 July ; 13(5): 1673–1683. doi:10.1016/j.nano.2017.03.002.

Effect of particle size on the biodistribution, toxicity, and efficacy of drug-loaded polymeric nanoparticles in chemoradiotherapy

Joseph M. Caster[1], **Stephanie K. Yu**[1], **Artish N. Patel**[1], **Nicole J. Newman**[1], **Zachary J. Lee**[1], **Samuel B. Warner**[1], **Kyle T. Wagner**[1], **Kyle C. Roche**[1], **Xi Tian**[1], **Yuanzeng Min**[1], and **Andrew Z. Wang**[1]

[1]University of North Carolina at Chapel Hill, Chapel Hill, NC 27599, USA

Abstract

Nanoparticle (NP) therapeutics can improve the therapeutic index of chemoradiotherapy (CRT). However, the effect of NP physical properties, such particle size, on CRT is unknown. To address this, we examined the effects of NP size on biodistribution, efficacy and toxicity in CRT. PEG-PLGA NPs (50, 100, 150 nm mean diameters) encapsulating wotrmannin (wtmn) or KU50019 were formulated. These NP formulations were potent radiosensitizers *in vitro* in HT29, SW480, and lovo rectal cancer lines. *In vivo*, the smallest particles avoided hepatic and splenic accumulation while more homogeneously penetrating tumor xenografts than larger particles. However, smaller particles were no more effective *in vivo*. Instead, there was a trend towards enhanced efficacy with medium sized NPs. The smallest KU60019 particles caused more small bowel toxicity than larger particles. Our results showed that particle size significantly affects nanotherapeutics' biodistrubtion and toxicity but does not support the conclusion that smaller particles are better for this clinical application.

Graphical Abstract

Sub50 nm drug-loaded NPs avoid hepatic clearance and more homogeneously distribute within tumors. However, they are no more efficacious and are associated with more small bowel toxicity than larger particles.

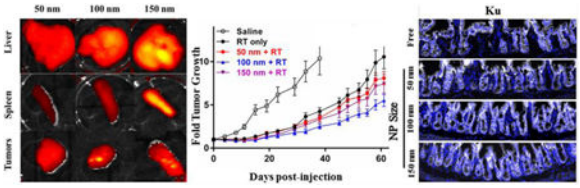

Corresponding Author: Joseph M Caster, MD. PhD., Lineberger Comprehensive Cancer Center, University of North Carolina at Chapel Hill, 101 Manning Drive, Chapel Hill North Carolina, 27599, 984-974-8718 (P), 984-974-8601 (F).

Keywords

Nanoparticle; Chemoradiotherapy; Nanoparticle radiosensitization; KU60019; Wortmannin

Background

Chemoradiotherapy (CRT) is a central treatment paradigm in the management of many solid cancers[1-3]. The generation of DNA double-strand breaks is thought to be one of the principle mechanisms of radiation-induced cell death and a number of potent DNA repair inhibitors have been developed. However, there is very little clinical experience combining these with radiation for fear of excess normal tissue toxicity when these drugs are administered systemically. Pre-clinical studies have demonstrated that nanoformulation of radiosensitizing drugs may be an effective way to accomplish this goal[4-9]. A number of potentially radiosensitizing nanotherapeutics have already been formulated and are being tested in the clinic[10-14]. It is worth noting, however, that none of these compounds were specifically engineered for use in CRT. Instead, they were optimized for chemotherapeutic drug delivery and are now being applied to CRT paradigms. The optimum particle characteristics for use in CRT, such as particle size, are currently unknown.

It is generally believed that “stealth” particles in the sub 50 nm range are desirable as drug delivery vehicles because they are more penetrating in tumors[15-18]. However, it is not clear that these characteristics are optimal for use in CRT. Radiation alters both tumor and normal tissue vasculature and it is unknown how this affects the therapeutic index of drug-loaded NPs[19-23]. We hypothesized that highly-penetrating small particles may increase toxicity in irradiated normal tissues and that the optimum therapeutic ratio might be achieved with larger particles (100-150nm). Understanding the relationship between particle size and therapeutic index will inform the optimal design of NP drug formulations for use in CRT.

We investigated the role of particle size in CRT by generating three populations of polymeric nanoparticles which differed only by size. These particles were approximately 50, 100, and 150 nm in mean diameter. We utilized two DNA repair inhibitors which target distinct DNA repair proteins as model drugs: the DNA-PK inhibitor wortmannin and the ATM inhibitor KU60019 as model drugs. Each NP encapsulated only one drug. We compared the antitumor efficacy of these formulations in three rectal cancer cell lines *in vitro*. We then compared the biodistribution, therapeutic efficacy, and toxicity of the particles when combined with raidation *in vivo* in mice with rectal tumor xenografts.

Methods

Materials

Wortmannin and KU60019 were purchased from Apex Bio (Houston Texas). Methoxypoly(ethylene glycol)-block-poly(lactic-co-glycolic acid) (mPEG-PLGA) with molecular weights of 2000:15000 (PEG(2K):PLGA(15K)) and 5000:1000 Da (PEG(5K):PLGA(10K)) were purchased from Akina (PolySciTech, West Lafayette, IN).

Rhodamine B-labeled PLGA with approximate molecular weight 30000 was purchased from Akina Inc. (PolySciTech, West Lafayette, IN). Poly(D,L-lactide) (PLA), ester terminated with average MW 18000-28000 was purchased from Sigma-Aldrich (St. Louis, MO). Acetonitrile (HPLC grade) and double distilled water (HPLC grade) were obtained from Sigma-Aldrich (St. Louis, MO).

Preparation of wortmannin or KU60019 nanoparticles

Polymeric nanoparticles encapsulating either wortmannin or KU60019 were generated utilizing a previously described nanoprecipitation method[6]. Briefly, polymers were dissolved in acetonitrile (ACN) (mPEG-PLGA 40 mg/ml, PLA 2 mg/ml). Drugs were also dissolved in ACN (2 mg/ml). Drug-polymer mixtures (1 ml) were then added dropwise to double deionized water (3 ml) over rapid stirring (1000 rpm). The mixture was then constantly stirred under vacuum at room temperature for 3 hours to allow self-assembly and evaporation of the organic solvent. Particles were then centrifuged for 15 min at 8000 × G in 30KDa cut-off centrifuge filters (Millipore, Billerica, MA). Particles were washed in 1× phosphate buffered saline (1 ml) followed by repeat centrifugation. After three washes particles were resuspended to desired concentrations in 1x phosphate buffered saline or tissue culture media.

Particle size was adjusted by altering the polymer compositions within the organic solvent mixtures. The smallest particles were obtained by adding 5 mg of 5000:10000 mPEG-PLGA and 500 μg (10%) KU60019 or wtmn. Intermediate sized particles were generated by adding 5 mg 2000:15000 mPEG-PLGA, 3 mg PLA, and 800 μg (10%) KU60019 or wtmn. The largest particles were generated by mixing 7 mg 2000:15000 mPEG-PLGA, 9 mg PLA, and 800 μg (5%) KU60019 or wtmn.

Preparation of Flamma Fluor-labeled nanoparticles

Flamme Fluor (FKR648)-labeled empty PEG-PLGA and PEG-PLGA-PLA particles were prepared via nanoprecipitation as above in the presence of 5% wt/wt FKR648-conjugated PLGA (AV 015, Akina Biosciences). FKR648-PLGA was diluted to 1 mg/ml, mixed with the solvent mixtures described above, and added dropwise to double deionized water. The solution was then continuously stirred under a vacuum in the dark for 3 hours and then particles were purified and washed 3 times as above. Empty particles were then resuspended in sterile PBS at desired concentrations. Incorporation efficiency was >95% for all particle sizes and was assessed by determining fluorescence intensity from the supernatant after filtration.

Characterization of nanoparticles

Purified particles encapsulating KU60019 or wtmn were characterized by transmission electron microscopy (TEM), dynamic light scattering, and aqueous electrophoresis. TEM images were captured using a Zeiss TEM 910 transmission electron microscope operated at 80 kV (Carl Zeiss Microscopy, LLC, Thornwood, NY) in the microscopy services laboratory core facility at the UNC school of medicine. Prior to TEM imaging, concentrated NP samples were diluted to 5 mg/ml in deionized water. A 5 μL sample of each was mixed with 5 μL 4% uranyl acetate aqueous solution before being added to a 400 mesh carbon-filmed

copper grid. Intensity-average diameter (Dh, also known as hydrodynamic diameter) and mean zeta potential (mean ζ) of nanodispersions were determined by dynamic light scattering and an aqueous electrophoresis method using a Zetasizer Nano ZS instrument (Malvern Inc, Warcestershire, UK). All measurements were based on the average of three separate measurements.

Drug loading determination

KU60019 and wtmn loading in polymeric nanoparticles was quantified using a Shimadzu SPD-M20A high-pressure liquid chromatography (HPLC) instrument (Shimadzu, Kyoto, Japan) equipped with a diode array detector at a GP-C18 reverse phase column (pore size = 120 Å, 4.6 × 150 mm, Sepax Technology, Newark, DE). A linear gradient from 10% ACN in water to 100% ACN was run over 15 min, followed by 100% ACN for 5 min, and finally 10% ACN for 5 min. Flow rate was 1 mL/min. Wtmn eluted with a retention time of 5.6 min and was read at a wavelength of 250 nm. KU60019 eluted with a retention time of 6.4 min and was detected at a wavelength of 230 nm. For preparation, 100 μL of purified particles was dissolved in 100 μL of ACN, vortexed vigorously, and stored over night at 4°C to allow complete dissolution of particles. Drug concentrations were determined by generating standard curves from 0-100 μM for each drug. Drug loading (wt/wt%) was calculated as (wt drug mg/wt polymer mg) × 100%. Encapsulation efficiency was calculated as (concentration drug in dissolved particles/concentration of drug in initial organic phase solution) × 100%.

In vitro drug release studies

Drug release rates were measured by placing 100 μL of purified particles diluted to 2.5 mg/ml into Slide-A-Lyzer MINI dialysis tubes with a molecular weight cut off of 10 kDa (Pierce, Rockford, IL) and subjected to dialysis against a large excess (4L) of PBS with gentle stirring at 37°C. At indicated times, whole samples were removed and dissolved as described above in ACN to allow disruption overnight. Drug concentrations were then determined using HPLC as above. Drug loading and encapsulation efficiency were determined at time 0 (immediately after purification). Drug release half-life ($T_{1/2}$) is defined as the time for half the encapsulated drug to be released and was calculated using GraphPad Prism software V4.0 (La Jolla, CA).

Cell Culture

Human rectal cancer cell lines HT29, SW480, and Lovo were obtained from the University of North Carolina tissue culture facility. HT29 and SW480 cells were cultured using DMEM F:12 media (Gibco, Thermo Fisher Scientific, Waitham, MA) supplemented with 10% (v/v) FBS and 1% penicillin/streptomycin. Lovo cells were cultured in DMEM F:12 media supplemented with 20% (v/v) FBS and 1% penicillin/streptomycin.

In vitro cytotoxicity

In vitro toxicities of different sized particles for KU60019 and wtmn were determined using MTS cell viability assays. Cells were plated in 96 well plates at densities of 10000 cells per well. Cells were then treated with varying concentrations of drug 24 hours later. For wtmn studies, drug was removed after 3 hours and cells were washed 3 times with sterile PBS and

then grown in fresh media for 48 hours at 37°C. For KU60019, drug was removed after 24 hours and cells were then washed and cultured as above. Cell viability was assessed using an MTS assay following manufacture's (Promega, Madison WI) instructions. Absorbance was recorded at 492 nm using a 96-well plate reader (Infinate 200 Pro, Tecan i-control). Relative cell survival was determined by dividing the intensity of each well by the average intensity obtained in wells containing cells treated with saline multiplied by 100.

In vitro clonogenic cell survival assays

In vitro radiosensitization effects of KU60019 and wtmn were determined using clonogenic cell survival assays. Cells were cultured at densities ranging from 100 to 100000 cells per dish for 24 hours. Media was then replaced with media containing varying concentrations of NP KU60019 (equivalent 2.5 μM for HT29 and SW480, 1.5 μM for Lovo) for 3 hours and then radiated with 0, 2, 4, 6, or 8 Gy of radiation. NP KU60019 was then left on for 21 additional hours for a total of 24 hours. Media was then removed and cells were washed three times with sterile PBS and then cultured in fresh media at 37°C for 12 days. For wtmn experiments, cells were treated with media containing NP wtmn (equivalent 20 μM for HT29 and SW480, 15 μM for Lovo) for 3 hours followed by the same doses of radiation. Cells were then washed 3 times with sterile PBS and cultured in fresh media at 37°C for 12 days. Cells were then fixed in a 4% (v/v) neutral buffered formalin solution with trypan blue. All colonies with more than 50 cells were then counted.

In vivo studies

Animals were maintained in the Center for Experimental Animal Studies (an AAA LAC-accredited experimental animal facility) at the University of North Carolina. All procedures involving animals were done in accordance with protocols approved by the University of North Carolina Institutional Animal Care and Use Committee and conformed to the Guide for the Care and Use of Laboratory Animals (NIH publication no. 86-23). C57bl/6J mice were obtained from Jackson Labs (Barr Harbor, ME). Athymic nude mice were obtained from UNC animal services core (Chapel Hill, NC).

In vivo biodistribution study

Nude mice were inoculated with HT29 xenografts (1×10^6 cells). Seven days after inoculation the average tumor size was $150mm^2$. The tumors were then treated with 3 daily doses of 5Gy radiation as above. Following the third fraction of radiation, animals were injected with saline or 165 mg/kg Flamma Fluor-labeled particles by IV tail vein injection. Following anesthetic overdose and decapitation, organs (heart, liver, spleen, tumor xenograft) were harvested at 1, 3, 6, 12, and 24 hours after injection for *ex vivo* imaging. Fluorescent images were obtained using and IVIS Living Image system (Caliper Life Science, Hopkiton, MA) equipped with an excitation filter of 640 nm and an emission filter of 680 nm in the small animal imaging facility at the UNC school of medicine. Region-of-interest values were recorded as photon flux in total photon count per cm^2 per steradian.

In vivo antitumor efficacy

Xenograft tumors were injected into the left flanks of male nude athymic mice (6-7 weeks old, 28-30 g). Mice were inoculated with 1×10^6 HT29 cells in a 1:1 mixture of FBS free DMEM F:12 media:matrigel mixture. The average tumor volume after 7 days was 200.0 mm^2. Mice were inoculated with 2.25×10^6 SW480 cells in in a 1:1 mixture of FBS free DMEM F:12 media/matrigel mixture. The average tumor volume after 10 days was 166.3 mm^2. For these experiments we utilized a clinically relevant fractionated radiation schedule with repeated dosing of NPs. On the first day of treatment (7 days after inoculation for HT29, 10 days after inoculation for SW480), animals were injected with saline, NP wtmn (0.07 mg/kg)), or NP KU60019 (0.5 mg/kg) via tail vein injection. Both doses were selected based on previous publications. Three hours after injection, tumors were irradiated at a dose of 5 Gy using a precision Xrad 320 (Precision X-ray Inc) operating at 320 KVp and 12.5 mA. The source-surface distance was 47 cm at a dose rate of 110 cGy/min. For radiation, the tumors were left exposed and mice were shielded with 4 mm of lead. On the second day, animals were treated with 5 Gy of radiation with no nanoparticle drug. On day 3, animals were again injected with saline or nanoparticles and then treated with 5 Gy radiation 3 hours later. To test the effects of particle size on chemotoxicity without radiation, a separate cohort of animals were treated with saline or NP formulations on days 1 and 3 with no radiation. Tumor volume was then assessed every 3 days via caliper measurements in two perpendicular directions. Tumor volume was calculated as $0.5 * x * y^2$, where x is the larger dimension and y is the smaller dimension. Animals were euthanized when the tumors reached greater than 20 mm in greatest dimension or when tumor volume measured greater than 3500 mm^2.

In vivo toxicity

We utilized histologic assessment of small bowel crypt density following CRT as a quantitative measure of gastrointestinal (GI) toxicity. The small bowel was selected as it is frequently the dose-limiting structure in pelvic/abdominal CRT. Tumor-free C57bl/J6 mice were treated with 3 daily doses (5 Gy each) of whole abdominal radiation preceded 3 hours earlier by saline or NP injections on days 1 and 3 (same treatment schedule as utilized *in vivo* tumor efficacy studies). Forty eight hours after the last fraction of radiation, animals were euthanized by CO2 overdose and distal iliums were harvested and fixed in 4% neutral buffered formalin solution overnight and then stored in 70% ethanol prior to being paraffin embedded and processed at the UNC Tissue core facility. Immunostainings of paraffin-embedded samples were performed according to standard procedure. Antigen retrieval was accomplished by boiling samples in Na-citrate buffer (10 mM, pH 6.0) for 20 min. Samples were incubated with rabbit anti-mouse EpCam antibody (1:100, Abcam). Stainings were visualized with Alexa 488-conjugated secondary goat antibodies (molecular probes) and nuclei were counterstained with DAPI (molecular probes).

The effects of particle size on the systemic toxicities of wtmn and KU60019 were assessed by analyzing blood counts (CBC with differential) and hepatotoxicity in tumor-free 8 week old C57bl/6J mice treated with the various sized particle formulations on days 1 and 3 without radiation. Blood was collected 48 hours after the last injection via cardiac puncture. Animals were anesthetized with a ketamine/xylazine solution prior to cardiac puncture

procedure. A 100 μL sample of whole blood was stored in EDTA-coated tubes at 5°C prior to analysis at the Animal Clinical Core Facility at the University of North Carolina. For hepatotoxicity, a 400 μL sample of whole blood was transferred to a serum separator tube and stored at room temperature for 30 minutes followed by centrifugation at 5000 × g for 10 min to separate plasma from the cellular components. Isolated plasma was then stored at 5°C prior to analysis at the Animal Clinical Core Facility at the University of North Carolina. Any samples that were pink in color (indicating hemolysis) after centrifugation were discarded as hemolysis can contaminate samples with non-hepatic sources of target enzymes. Sample readings which were+/- more than 3 times the SD of the mean were also presumed to be hemolyzed and discarded (N=2 from saline treated animals, and 0-1 from all other groups).

Statistical Analysis

In vitro cytotoxicity (MTS assays) was assessed using two-way analysis of variance (ANOVA) with variables of particle size and drug concentration using Prism software (Carlesbad, CA). Clonogenic survival assays were plotted in a linear quadratic fashion calculated using CS Cal clonogenic survival calculation software pack. Hematologic and hepatotoxicity were assessed using one way ANOVA of particle size. Post-hoc analyses were performed using Tukey's T test when significant main effects were identified. In vivo tumor growth was assessed using AUC analysis (R software).

Results

Generation of distinct size populations of polymeric nanoparticles

We engineered NP formulations of KU60019 and wtmn with different mean sizes ranging from 50-150 nm by altering polymeric compositions. This method produced monodisperse populations of NPs with PDIs of less than 0.1. Figure 1 provides a schematic representation of the different NP formulations. Table 1 shows the polymeric formulations used to generate the different populations as well as mean particle sizes and PDIs. The top panels of figure 2 show representative TEM images of wtmn and KU60019 nanoformulations. Size distribution plots (figure 2, middle panels) demonstrate that there is virtually no overlap between the largest and smallest sized particles.

To determine the effect of particle size on therapeutic efficacy, it was necessary to engineer varying sized particles with similar release rates. Larger particles tend to have faster release rates and we offset this effect by increasing the hydrophobicity of the larger sized particles[24]. As shown in the bottom panels of figure 2, the three size populations had similar release rates for both drugs.

In vitro efficacy

To determine the efficacy of different sized NPs in CRT, we first compared the *in vitro* cytotoxicity of the various sized particles in HT29, SW480, and Lovo rectal cancer cells. Nanoformulations of wtmn and KU60019 showed comparable levels of cytoxicity in the absence of radiation (figure 3 top panels). The IC90 for both drugs was between 10 and 20

μM in HT29 and SW480 cells and between 5 and 10 μM in Lovo cells. There was no effect of particle size on *in vitro* cytotoxicity.

The three cell lines were then exposed to varying doses of radiation following NP drug treatment (figure 3 bottom panels). Wtmn particles potently sensitized all three cell lines to radiation at doses corresponding to roughly the IC90 (20 μM for HT29 and SW480, 10 μM for lovo). KU60019 particles were exquisitely potent radiosensitizers at doses corresponding to $1/10^{th}$ the IC90. There was no significant effect of particle size for either drug.

In vivo biodistribution

We tested the effect of particle size on biodistribution by administering particles labeled with a fluorescent tag and imaging organs (heart, liver, spleen, tumor xenograft) harvested at 1, 3, 6, 12, and 24 hours after administration of labeled particles. Figure 4 shows representative images of organs normalized to unlabeled control background. The largest particles rapidly accumulated in the liver and spleen. Medium sized particles accumulated more in the liver and spleen than the smallest particles but less than the largest ones. Particles of all sizes accumulated within tumors at similar overall average intensity levels. However, the signal was most homogenous with the 50 nm particles. Larger particles produced a more punctate pattern, consistent with accumulation in the perivascular space[17].

In vivo antitumor efficacy

To compare the *in vivo* efficacy of different size nanoparticle formulations, animals with HT29 or SW480 xenografts were treated with equivalent doses of different sized NPs. We tested the antitumor efficacy of particles as both chemotherapeutics (figure 5) and as radiosensitizers (figure 6).

All formulations had minimal effect on tumor growth in the absence of radiation (figure 5). In HT29 xenografts, wtmn particles delayed tumor growth compared to saline ($P<0.04$) but this effect was relatively small and was not affected by particle size. There was no significant tumor growth delay in any other tumor/drug combinations in the absence of radiation.

In contrast, formulations of both drugs were potently radiosensitizing to both tumor histologies (figure 6). With wtmn particles, all three particle sizes delayed HT29 tumor growth and there was no significant difference between the three particle sizes. In SW480-bearing mice, 100 nm wtmn particles produced significantly more radiosensitization than smaller or larger particles ($P<0.04$). There were no statistically significant effects of particle size in animals treated with KU60019 particles although there was a strong trend ($P<0.10$) towards improved sensitization with 100 nm particles in both xenograft models. In no instances did treatment with the smallest particles (50 nm) result in superior antitumor efficacy than larger particles *in vivo*.

In vivo toxicity

GI toxicity was quantified by measuring small bowel crypt density 48 hours after the third fraction of whole abdominal radiation (figure 7). Radiation with free drugs produced a

marked decrease in crypt density. Nanoformulation largely attenuated the synergistic toxicity between drug and radiation. The smallest KU60019 particles were more toxic than medium or large particles. There was no significant effect of particle size with wtmn NPs.

Systemic effects of each drug were assessed by measuring hematologic and hepatic toxicities in animals 48 hours after treatment with two injections of NPs (days 1 and 3) without radiation (table 2). Hepatotoxicity is one of the limiting toxicities of wtmn. NP formulation largely attenuated the hepatotoxic effects of wtmn. There was a trend towards greater AST and ALT levels in mice treated with NP wtmn compared to saline but this was not significant ($P=0.23$). Treatment with NP KU60019 did significantly increase plasma AST concentrations compared to saline ($P<0.05$) but there was no significant effect of particle size on the hepatoxicity of either drug.

We also measured changes in peripheral blood counts with drug treatment by assessing complete blood counts (CBCs). Wtmn particles caused significant decreases in white blood cell (WBC) though this effect was relatively small and there was no effect of particle size. KU60019 particles had no effect on any CBC variables.

Discussion

Multiple studies have demonstrated the potential for NP formulations of radiosensitizing drugs to improve the therapeutic ratio of CRT and several compounds are currently being tested in clinical trials. Despite this, none have been specifically formulated for CRT and very little is known about the optimal particle characteristics for use in CRT. In this study, we compared the biodistribution, efficacy, and toxicity of particles ranging from 50-150 nm in diameter. This size range is consistent with that of polymeric particles currently in clinical development[14]. We confirmed that sub50 nm particles more homogenously penetrate tumors than larger particles. However, we were unable to demonstrate any therapeutic advantage to utilizing such small particles with radiation. Instead, we observed greater GI toxicity with the smallest particles and a trend towards improved efficacy with 100 nm particles. Our results suggest that engineering sub50 nm particles may not be optimal for use in CRT applications.

To our knowledge, this is the first study to address the effects of particle size on both therapeutic efficacy and toxicity with radiation. We confirmed that 50 nm particles more homogenously penetrate tumors than larger particles[16, 17]. It has been speculated that these characteristics make small particles more desirable drug delivery vectors. However, we were unable to demonstrate any therapeutic advantage to utilizing the smallest particles with radiation. Instead, we observed more radiosensitization with medium-sized particles. Differences in tumor penetration could partially explain this observation. Indirectly ionizing radiation is dependent upon adequate oxygenation in the immediate vicinity of the resulting molecular damage[25]. By homogenously penetrating tumors, the smallest particles are indiscriminately localizing drug in oxygen-rich and hypoxic regions. In contrast, larger particles accumulate within the perivascular space thus concentrating drug within the oxygenated tumor regions where radiosensitizers should be most effective.

Our results also support our hypothesis that very small particles may cause more normal tissue toxicity when combined with radiation. Under physiologic (unirradiated) conditions, 30-50 nm particles are too large to extravasate highly ordered normal tissue capillaries. However, radiation acutely increases the permeability of normal tissue capillaries[22, 26-28]. The smallest KU60019 particles significantly increased intestinal toxicity with radiation whereas no increased toxicity was observed with any of the larger particles. These data suggest that radiation selectively increases the vascular permeability of very small, but not larger particles. Thus, sub50 nm particles may have a lower therapeutic index than larger particles when combined with radiation.

Particle size and drug release kinetics are two of the most important NP properties which can affect therapeutic efficacy[29, 30]. Therefore, it was necessary to engineer particles with similar drug-release kinetics to try to isolate the effects of particle size on efficacy and toxicity. It is worth noting that it is very difficult to engineer particles that differ by only a single variable. If all other variables are held constant, drug release is inherently faster from larger particles as the larger pore sizes are more conducive to passive diffusion. We slowed the drug release rates of larger particles by increasing the hydrophobicity of the particle core. While this adequately controls for drug-release kinetics, these particles do have different physiochemical properties and it is not entirely clear how these differences could affect our results.

There are several other limitations to our study that should be considered. While we utilized a fractionated treatment regimen to mimic clinical delivery of CRT, this only consisted of 3 fractions of radiation and 2 injections of drug. Clinical treatment paradigms occur over much more protracted courses (20-30 fractions over 4-6 weeks). Additionally, we utilized xenograft tumor models which differ from native tumors, particularly in terms of tumor microenvironment[31]. This may limit the generalizability of our results to spontaneously-occurring human tumors.

In conclusion, our study has demonstrated that polymeric NPs encapsulating radiosensitizing drugs in clinically relevant size ranges (50-150 nm) are potent radiosensitizers and well tolerated. While very small particles more homogenously penetrate tumors, they are no more efficacious and if anything may be more toxic than larger particles when combined with radiation. Our results suggest that in contrast to chemotherapy-only applications, very small (sub50 nm) particles may not be optimal when combined with radiation therapy.

Acknowledgments

This work was supported by National Institutes of Health Grant RO1CA1787148.

References

1. Adelstein DJ, Li Y, Adams GL, Wagner H Jr, Kish JA, Ensley JF, et al. An intergroup phase III comparison of standard radiation therapy and two schedules of concurrent chemoradiotherapy in patients with unresectable squamous cell head and neck cancer. J Clin Oncol. 2003; 21:92–8. [PubMed: 12506176]

2. Bosset JF, Calais G, Mineur L, Maingon P, Radosevic-Jelic L, Daban A, et al. Enhanced tumorocidal effect of chemotherapy with preoperative radiotherapy for rectal cancer: preliminary results--EORTC 22921. J Clin Oncol. 2005; 23:5620–7. [PubMed: 16009958]

3. De Caluwe L, Van Nieuwenhove Y, Ceelen WP. Preoperative chemoradiation versus radiation alone for stage II and III resectable rectal cancer. Cochrane Database Syst Rev. 2013:CD006041. [PubMed: 23450565]

4. Karve S, Werner ME, Sukumar R, Cummings ND, Copp JA, Wang EC, et al. Revival of the abandoned therapeutic wortmannin by nanoparticle drug delivery. Proc Natl Acad Sci U S A. 2012; 109:8230–5. [PubMed: 22547809]

5. Tian X, Lara H, Wagner KT, Saripalli S, Hyder SN, Foote M, et al. Improving DNA double-strand repair inhibitor KU55933 therapeutic index in cancer radiotherapy using nanoparticle drug delivery. Nanoscale. 2015; 7:20211–9. [PubMed: 26575637]

6. Au KM, Min Y, Tian X, Zhang L, Perello V, Caster JM, et al. Improving Cancer Chemoradiotherapy Treatment by Dual Controlled Release of Wortmannin and Docetaxel in Polymeric Nanoparticles. ACS Nano. 2015; 9:8976–96. [PubMed: 26267360]

7. Kim K, Oh KS, Park DY, Lee JY, Lee BS, Kim IS, et al. Doxorubicin/gold-loaded core/shell nanoparticles for combination therapy to treat cancer through the enhanced tumor targeting. J Control Release. 2016; 228:141–9. [PubMed: 26970205]

8. Jung J, Park SJ, Chung HK, Kang HW, Lee SW, Seo MH, et al. Polymeric nanoparticles containing taxanes enhance chemoradiotherapeutic efficacy in non-small cell lung cancer. Int J Radiat Oncol Biol Phys. 2012; 84:e77–83. [PubMed: 22795728]

9. Wang AZ, Yuet K, Zhang L, Gu FX, Huynh-Le M, Radovic-Moreno AF, et al. ChemoRad nanoparticles: a novel multifunctional nanoparticle platform for targeted delivery of concurrent chemoradiation. Nanomedicine (Lond). 2010; 5:361–8. [PubMed: 20394530]

10. Dipetrillo T, Suntharalingam M, Ng T, Fontaine J, Horiba N, Oldenburg N, et al. Neoadjuvant paclitaxel poliglumex, cisplatin, and radiation for esophageal cancer: a phase 2 trial. Am J Clin Oncol. 2012; 35:64–7. [PubMed: 21297434]

11. Hasegawa T, Futamura Y, Horiba A, Yoshida T, Suzuki T, Kato T, et al. A phase II study of nabpaclitaxel plus carboplatin in combination with thoracic radiation in patients with locally advanced non-small-cell lung cancer. J Radiat Res. 2016; 57:50–4. [PubMed: 26442970]

12. Nardone L, Diletto B, De Santis MC, GR DA, Belli P, Bufi E, et al. Primary systemic treatment and concomitant low dose radiotherapy for breast cancer: final results of a prospective phase II study. Breast. 2014; 23:597–602. [PubMed: 24998453]

13. Tsoutsou PG, Froudarakis ME, Bouros D, Koukourakis MI. Hypofractionated/accelerated radiotherapy with cytoprotection (HypoARC) combined with vinorelbine and liposomal doxorubicin for locally advanced non-small cell lung cancer (NSCLC). Anticancer Res. 2008; 28:1349–54. [PubMed: 18505077]

14. Min Y, Caster JM, Eblan MJ, Wang AZ. Clinical Translation of Nanomedicine. Chem Rev. 2015; 115:11147–90. [PubMed: 26088284]

15. Cabral H, Matsumoto Y, Mizuno K, Chen Q, Murakami M, Kimura M, et al. Accumulation of sub-100 nm polymeric micelles in poorly permeable tumours depends on size. Nat Nanotechnol. 2011; 6:815–23. [PubMed: 22020122]

16. Lee H, Fonge H, Hoang B, Reilly RM, Allen C. The effects of particle size and molecular targeting on the intratumoral and subcellular distribution of polymeric nanoparticles. Mol Pharm. 2010; 7:1195–208. [PubMed: 20476759]

17. Matsumoto Y, Nichols JW, Toh K, Nomoto T, Cabral H, Miura Y, et al. Vascular bursts enhance permeability of tumour blood vessels and improve nanoparticle delivery. Nat Nanotechnol. 2016; 11:533–8. [PubMed: 26878143]

18. Schadlich A, Caysa H, Mueller T, Tenambergen F, Rose C, Gopferich A, et al. Tumor accumulation of NIR fluorescent PEG-PLA nanoparticles: impact of particle size and human xenograft tumor model. ACS Nano. 2011; 5:8710–20. [PubMed: 21970766]

19. Park KR, Monsky WL, Lee CG, Song CH, Kim DH, Jain RK, et al. Mast Cells Contribute to Radiation-Induced Vascular Hyperpermeability. Radiat Res. 2016; 185:182–9. [PubMed: 26771172]

20. Li C, Ke S, Wu QP, Tansey W, Hunter N, Buchmiller LM, et al. Tumor irradiation enhances the tumor-specific distribution of poly(L-glutamic acid)-conjugated paclitaxel and its antitumor efficacy. Clin Cancer Res. 2000; 6:2829–34. [PubMed: 10914731]
21. Jin X, Liang B, Chen Z, Liu X, Zhang Z. The dynamic changes of capillary permeability and upregulation of VEGF in rats following radiation-induced brain injury. Microcirculation. 2014; 21:171–7. [PubMed: 25279427]
22. Willoughby DA. Pharmacological aspects of the vascular permeability changes in the rat's intestine following abdominal radiation. Br J Radiol. 1960; 33:515–9. [PubMed: 13844999]
23. Ng QS, Goh V, Milner J, Padhani AR, Saunders MI, Hoskin PJ. Acute tumor vascular effects following fractionated radiotherapy in human lung cancer: In vivo whole tumor assessment using volumetric perfusion computed tomography. Int J Radiat Oncol Biol Phys. 2007; 67:417–24. [PubMed: 17236965]
24. Andreani T, Fangueiro JF, Jose S, Santini A, Silva AM, Souto EB. Hydrophilic Polymers for Modified-Release Nanoparticles: A Review of Mathematical Modelling for Pharmacokinetic Analysis. Curr Pharm Des. 2015; 21:3090–6. [PubMed: 26027576]
25. Palcic B, Skarsgard LD. Reduced oxygen enhancement ratio at low doses of ionizing radiation. Radiat Res. 1984; 100:328–39. [PubMed: 6494444]
26. Evans ML, Graham MM, Mahler PA, Rasey JS. Changes in vascular permeability following thorax irradiation in the rat. Radiat Res. 1986; 107:262–71. [PubMed: 3749461]
27. Song CW, Anderson RS, Tabachnick J. Early effects of beta irradiation on dermal vascular permeability to plasma proteins. Radiat Res. 1966; 27:604–15. [PubMed: 5934822]
28. Krishnan L, Krishnan EC, Jewell WR. Immediate effect of irradiation on microvasculature. Int J Radiat Oncol Biol Phys. 1988; 15:147–50. [PubMed: 3391811]
29. Yoon HY, Koo H, Choi KY, Chan Kwon I, Choi K, Park JH, et al. Photo-crosslinked hyaluronic acid nanoparticles with improved stability for in vivo tumor-targeted drug delivery. Biomaterials. 2013; 34:5273–80. [PubMed: 23591396]
30. Wang J, Sui M, Fan W. Nanoparticles for tumor targeted therapies and their pharmacokinetics. Curr Drug Metab. 2010; 11:129–41. [PubMed: 20359289]
31. Richmond A, Su Y. Mouse xenograft models vs GEM models for human cancer therapeutics. Dis Model Mech. 2008; 1:78–82. [PubMed: 19048064]

List of abbreviations

ACN	acetonitrile
ANOVA	analysis of variance
CBC	complete blood count
CRT	chemoradiotherapy
GI	gastrointestinal
Hb	hemoglobin
HCT	hematocrit
mPEG-PLGA	methoxy-poly(ethylene glycol)-block-poly(lactic-co-glycolic acid)
NP	nanoparticle
PLA	poly(D,L-lactide)
WBC	white blood cell

wtmn	wortmannin

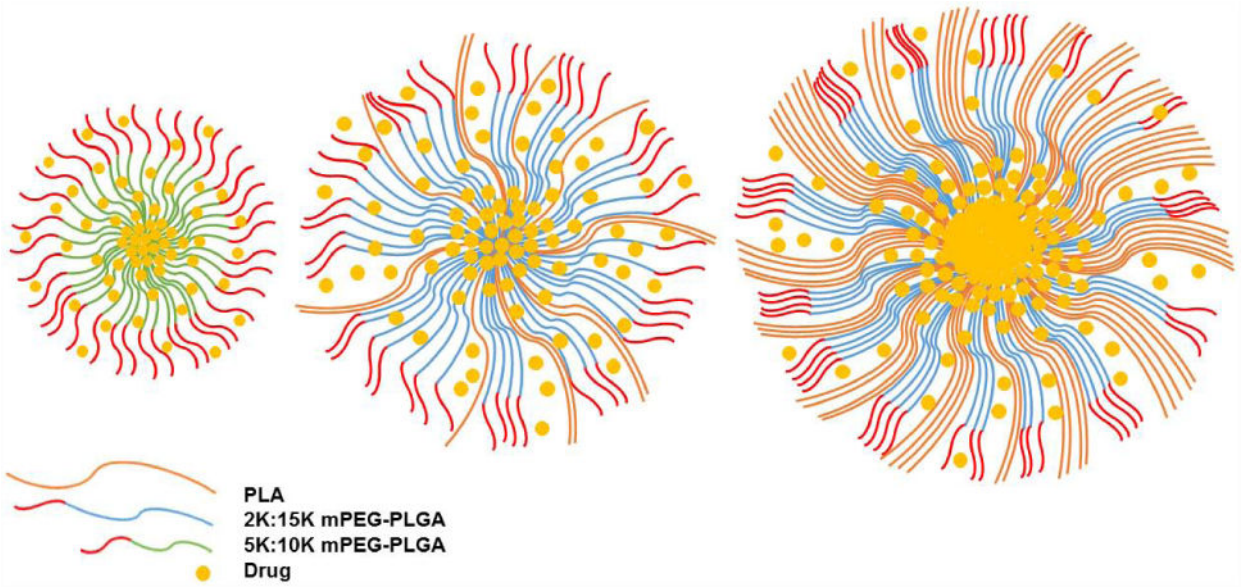

Figure 1.
Schematic representation of polymeric NP formulations.

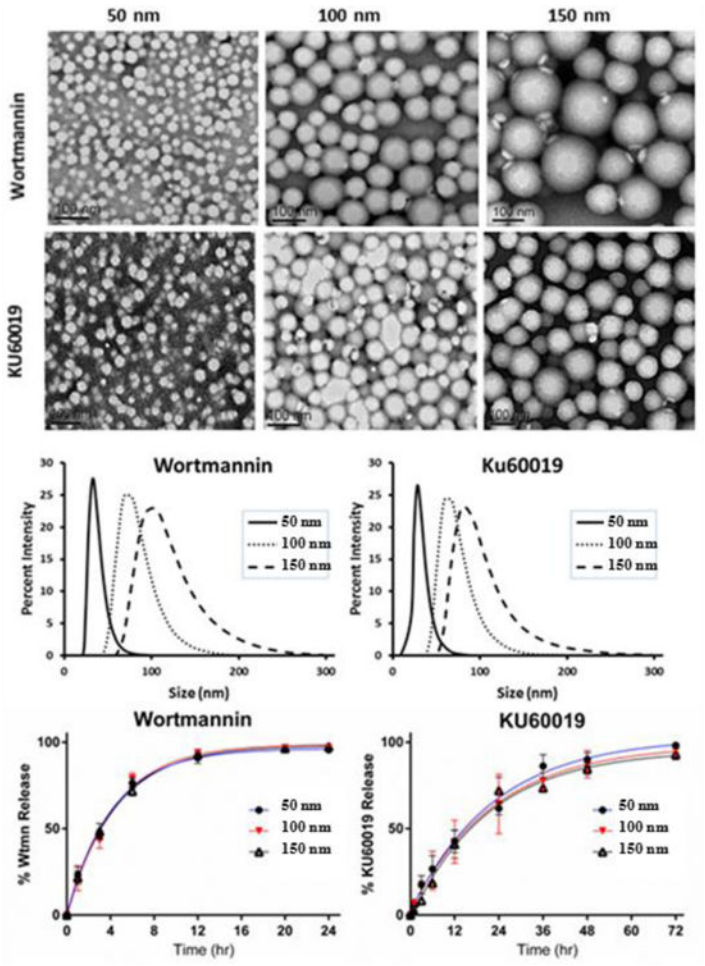

Figure 2. Nanoparticle Characteristics

Transmission electron microscopic images of the various sized NP formulations (top panels, 50 nm left, 100 nm middle, 150 nm right). Particle size distribution plots (middle panels) demonstrating the relative distribution of particle sizes for each particle population. Drug release curves for wtmn (left) and KU60019 particles (bottom panels).

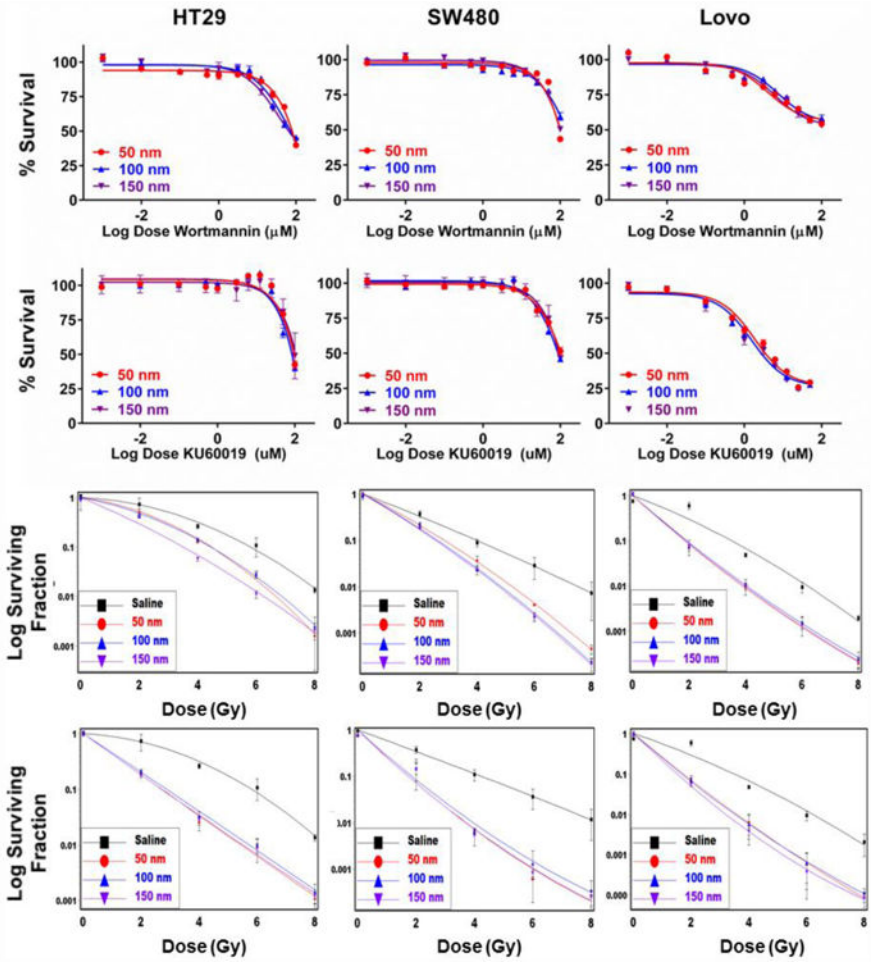

Figure 3. ***In vitro*** **efficacy of drug-loaded NPs**

Toxicity of drug-loaded particles without radiation in three rectal cancer cell lines as assessed using MTS assays (top 2 rows, HT29 left, SW480 middle, Lovo right). Y-axis shows the log of drug dose (wtmn top, KU60019 bottom) in micromolar. Radiosensitization of rectal cancer cell lines by polymeric wtmn and KU60019 particles (bottom 2 rows).

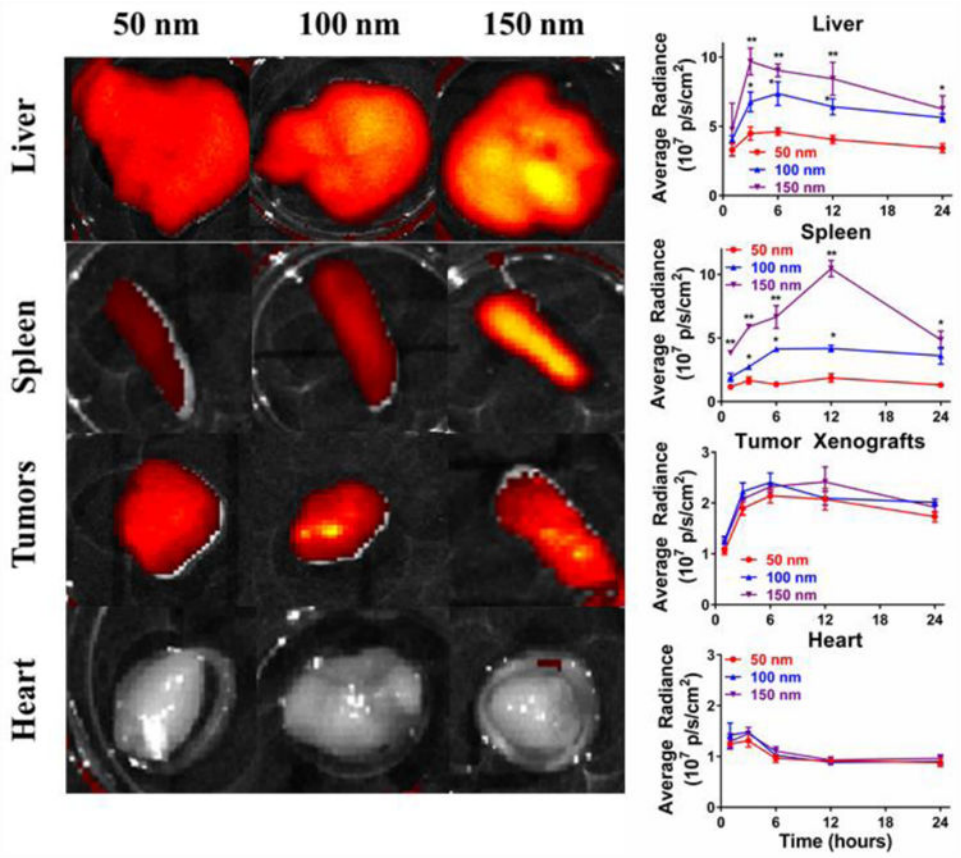

Figure 4. Effect of particle size on in vivo biodistribution

Background-normalized images of various organs harvested 6 hours after *in vivo* administration of fluorescent-labeled NPs (50 nm far left, 100 nm middle, 150 nm right). Far right column shows the accumulation of particles in the different organs at diferent times over 24 hours. * significantly more than 50 nm. ** significantly more than all other groups.

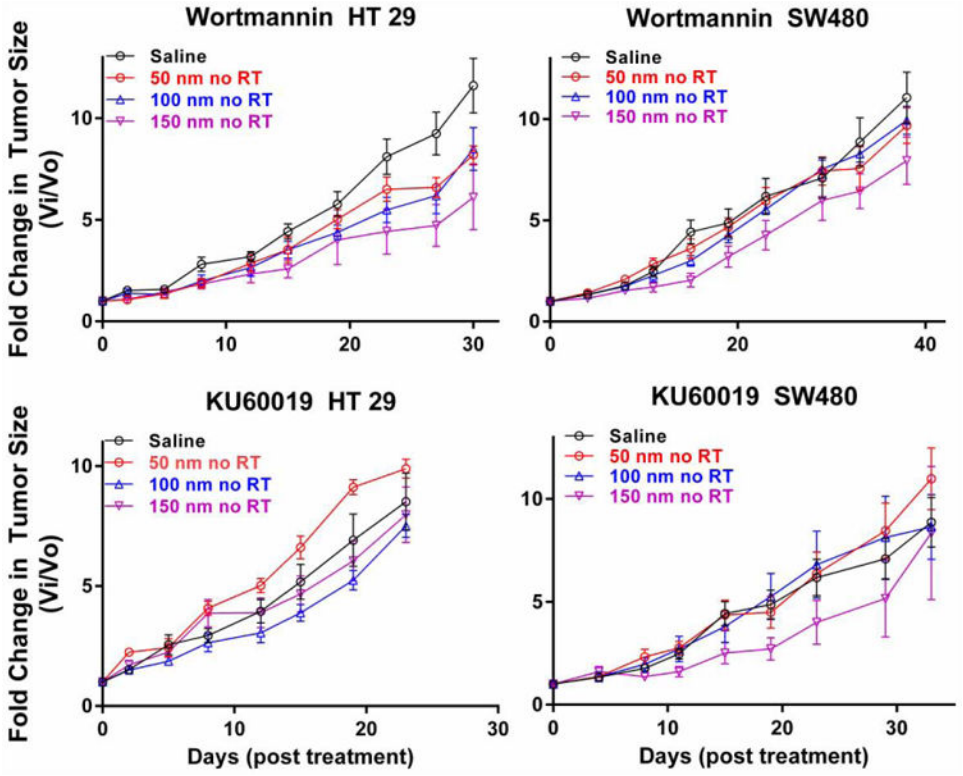

Figure 5. In vivo efficacy of drug-loaded NPs without radiation

Tumor growth curves of animals bearing HT29 (left panels) or SW480 xenografts (right panels) treated with wtmn (top panels) or KU60019 (bottom panels) NPs. Open black circles represent saline treated controls. Red open circles represent animals treated with 50 nm particles. Blue open triangles represent animals treated with 100 nm particles. Open purple triangles represent animals treated with 150 nm particles.

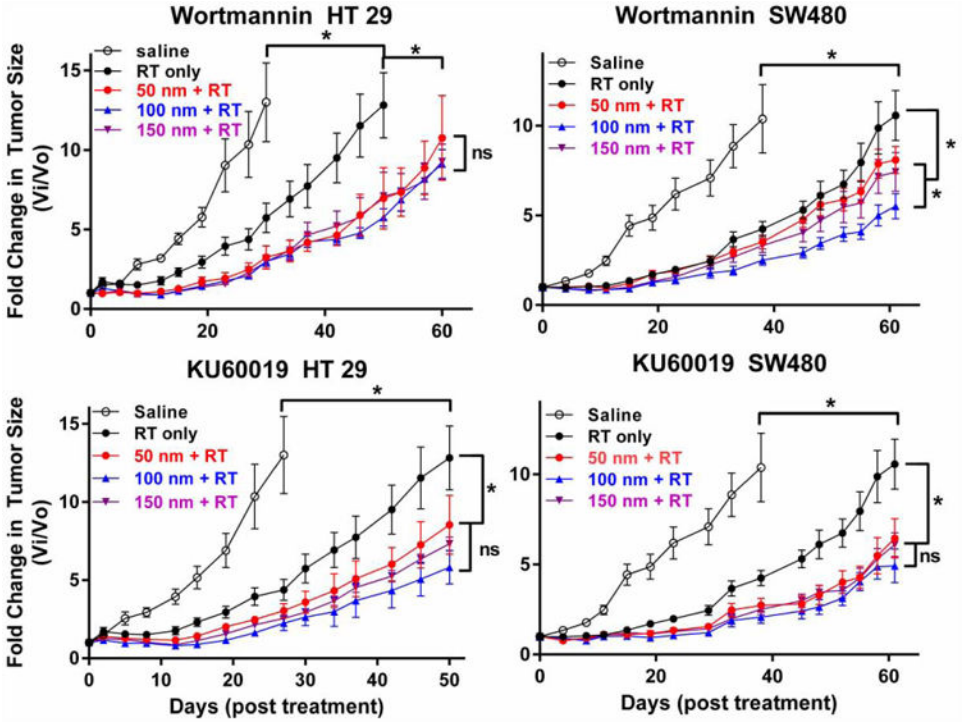

Figure 6. Effect of particle size on in vivo radiosensitization

Tumor growth curves of animals bearing HT29 (left panels) or SW480 xenografts (right panels) treated with wtmn (top panels) or KU60019 (bottom panels) NPs. Open black circles represent saline treated controls (no radiation). Closed black circles represent saline injected animals treated with radiation. Closed red circles represent animals treated with radiation and 50 nm particles. Closed blue triangles represent animals treated with 100 nm particles and radiation. Closed purple triangles represent animals treated with 150 nm particles and radiation. * significantly different from indicated groups. NS non-significant.

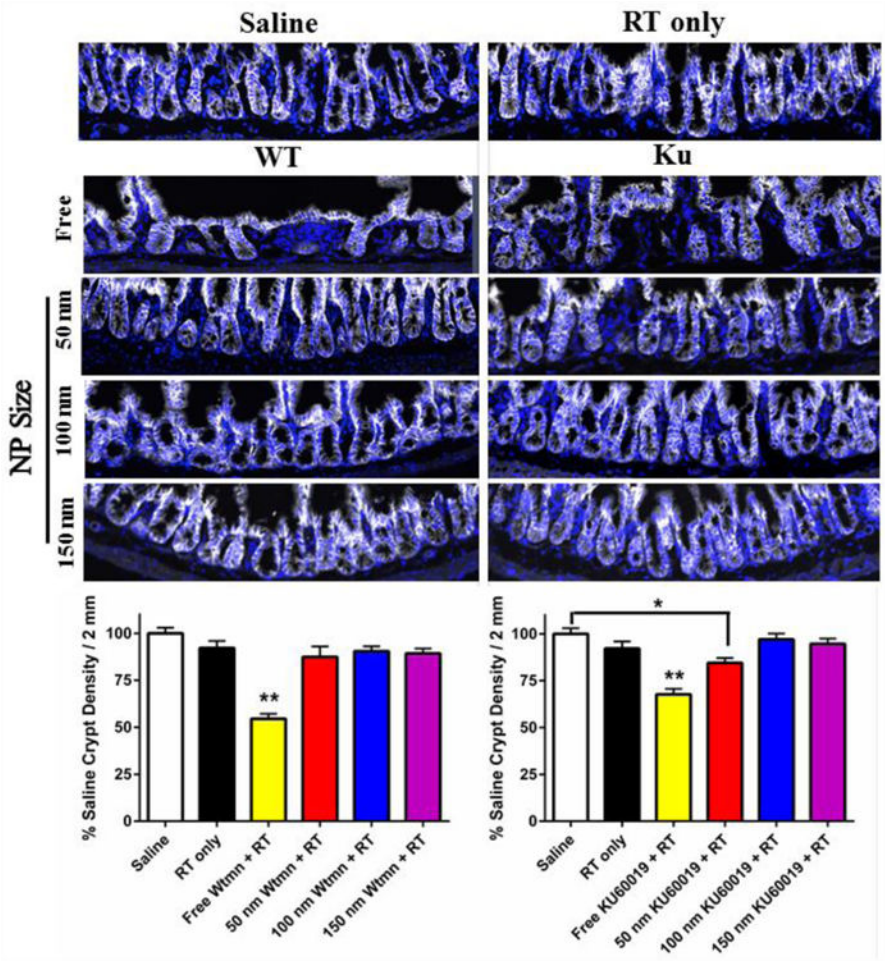

Figure 7. Effects of particle size on small bowel toxicity

Confocal microscopic slides of EpiCAM stained terminal ilial sections of animals treated with saline or radiation only (top lines), parenteral (free) drugs (second row), or various sized wtmn (left) or KU60019 (right) NPs. Quantified data is graphically shown in bottom panels. * significantly different from indicated groups. ** significantly different from all other groups.

Table 1

Polymeric NP composition and physical characteristics.

Formulation	Mean Diameter	PDI
5K:10K PEG-PLGA 10% Wtmn	48.4 +/- 1.1 nm	0.07 +/- 0.02
2K:15K PEG-PLGA 38% PLA 10% Wtmn	101.5 +/- 2.1 nm	0.06 +/- 0.02
2K:15K PEG-PLGA 56% PLA 5% Wtmn	147.3 +/- 2.4 nm	0.08 +/- 0.04
5K:10K PEG-PLGA 10% KU60019	44.3 +/- 0.9 nm	0.07 +/- 0.03
2K:15K PEG-PLGA 38% PLA 10% KU60019	94.6 +/- 1.8 nm	0.08 +/- 0.02
2K:15K PEG-PLGA 56% PLA 5% KU60019	138 +/- 2.4	0.09 +/- 0.03

Table 2

Effects of particle size on *in vivo* hepatic and hematologic toxicities

Plasma levels of the liver enzymes AST and ALT are show in the top of the table for wtmn (left half) and KU60019 (right half). Peripheral blood values for specific hematologic values (hemoglobin (Hb), hematocrit (HCT), red blood cells (RBC), white blood cells (WBC), lymphocytes, granulocytes, and monocytes.

	Wortmannin				**KU60019**			
Liver Function								
	AST	ALT			AST	ALT		
Normal Range	30-60 U/L	30-60 U/L			30-60 U/L	30-60 U/L		
Saline	57.5 +/-6.2	36.8 +/- 3.1			57.5 +/-6.2	36.8 +/- 3.1		
50 nm	76.3 +/-5.6	41.3 +/- 4.0			77.6 +/-5.1*	33.6 +/- 2.2		
100 nm	71.3 +/-4.0	40.1 +/- 2.0			80.0 +/-5.9*	39.6 +/- 1.3		
150 nm	69.7 +/-5.6	44.4 +/- 2.7			81.7 +/-6.2*	37.2 +/- 1.3		
Hematologi c Profile								
	Hb	Hct	RBC		Hb	Hct	RBC	
Normal Range	10.1-16.1 g/dL	32.8-48%	6.5-10.1 10^6/μL		10.1-16.1 g/dL	32.8-48%	6.5-10.1 10^6/μL	
Saline	15.6 +/-0.2	46.6 +/- 0.7	9.7 +/- 0.1		15.6 +/-0.2	46.6 +/- 0.7	9.7 +/- 0.1	
50 nm	15.8 +/-0.4	45.9 +/- 0.8	9.8 +/- 0.2		15.4 +/-0.2	45.2 +/- 1.0	9.6 +/- 0.2	
100 nm	16.0 +/-0.3	46.9 +/- 0.7	9.9 +/- 0.2		15.7 +/-0.3	46.8 +/- 1.1	9.8 +/- 0.2	
150 nm	15.8 +/-0.4	46.1 +/- 0.5	9.6 +/- 0.2		15.2 +/-0.2	45.3 +/- 0.8	9.5 +/- 0.2	
	WBC	Lymphocytes	Granulocytes	Monocytes	WBC	Lymphocytes	Granulocytes	Monocytes
Normal Range	2.6-10.1 10^3/μL	1.3-8.4 10^3/μL	0.4-2.0 10^3/μL	0-0.3	2.6-10.1 10^3/μL	1.3-8.4 10^3/μL	0.4-2.0 10^3/μL	0-0.3 10^3/μL
Saline	5.5 +/-0.6	4.5 +/- 0.4	0.6 +/- 0.2	0.5 +/- 0.1	5.5 +/-0.6	4.5 +/- 0.4	0.6 +/- 0.2	0.5 +/- 0.1
50 nm	2.8 +/-0.8*	2.2 +/- 0.9*	0.2 +/- 0.1	0.3 +/-0.1*	4.3 +/-0.4	3.7 +/- 0.3	0.4 +/- 0.1	0.3 +/- 0.6

	Wortmannin			KU60019			
100 nm	2.9 +/-0.6*	2.6 +/- 0.6*	0.1 +/- 0.1	0.2 +/-0.1*	3.8 +/-0.5	3.3 +/- 0.4	0.2 +/- 0.1	0.3 +/- 0.1
150 nm	3.0 +/-0.8*	2.5 +/- 0.7*	0.2 +/- 0.1	0.3 +/-0.1*	4.1 +/-0.5	3.6 +/- 0.5	0.2 +/- 0.1	0.3 +/- 0.1

* significantly different from saline-treated controls.